

THE HH34 JET/COUNTERJET SYSTEM AT 1.5 AND 4.5 μm

A. C. Raga¹, B. Reipurth², and A. Noriega-Crespo³

Received October 29 2018; accepted February 13 2019

ABSTRACT

We present a (previously unpublished) 1.5 μm archival HST image of the HH 34 Herbig-Haro jet, in which the northern counterjet is seen at an unprecedented angular resolution of $\approx 0.1''$ (this counterjet had only been imaged previously at lower resolution with Spitzer). The jet/counterjet structure observed in this image shows evidence of low-amplitude, point-symmetric deviations from the outflow axis, indicating the presence of a precession in the ejection direction. We use the ratios between the 1.5 and 4.5 μm intensities of the emitting knots (from the HST image and from a previously published 4.5 μm Spitzer image) to obtain an estimate of the spatial dependence of the optical extinction to the HH 34 jet/counterjet system. We find evidence for extinction from a central, dense core surrounding the outflow source and from a more extended region in the foreground of the HH 34 counterjet.

RESUMEN

Presentamos una imagen del chorro Herbig-Haro HH 34 (inédita) a 1.5 μm del archivo del HST, en la que el contrachorro norte se detecta con una resolución angular sin precedentes de $\approx 0.1''$ (las únicas imágenes previas de este contrachorro, obtenidas con el Spitzer, tienen una menor resolución). La estructura de chorro/contrachorro observada en esta imagen muestra evidencia de desviaciones de baja amplitud, con simetría de punto con respecto al eje del flujo, e indica la presencia de una precesión en la dirección de la expulsión. Usamos cocientes entre los flujos a 1.5 y 4.5 μm de los nudos emisores (obtenidos de la imagen del HST y de una imagen a 4.5 μm del Spitzer publicada previamente) para obtener una estimación de la dependencia espacial de la extinción óptica del sistema chorro/contrachorro HH 34. Encontramos evidencia de extinción debida a un núcleo denso rodeando a la fuente del flujo y a una zona más extendida situada enfrente del contrachorro de HH 34.

Key Words: Herbig-Haro objects — ISM: individual objects (HH34) — ISM: jets and outflows — ISM: kinematics and dynamics — stars: formation — stars: winds, outflows

1. INTRODUCTION

Since its discovery, the HH 34 jet has been one of the finest, brightest, and best collimated HH jets known to emanate from a young star. Early studies established the basic characteristics of the jet, showing that the jet moves out of a compact cloud core in the L1641 cloud in Orion (Reipurth et al. 1986, Bührke et al. 1988, Raga & Mateo 1988, Reipurth & Heathcote 1992).

A series of distant bow shocks have been discovered both to the south and the north, showing that HH 34 comprises a giant HH flow (Bally & Devine

1994), modeled by Cabrit & Raga (2000) and Masciadri et al. (2002). At the here adopted distance of 400 pc (Kounkel et al. 2017, Menten et al. 2007), the total projected extent of the HH complex is 2.5 pc.

The source is an embedded Class I protostar with a total luminosity of 21 L_{\odot} (value from Reipurth et al. 1993, but converted to a distance of 400 pc); the source was detected in the radio continuum by Rodríguez & Reipurth (1996) and Rodríguez et al. (2014). The HH 34 source is surrounded by a molecular cloud core, which has been studied by Stapelfeldt & Scoville (1993), Davis & Dent (1993), and Anglada et al. (1995). As the jet moves out from the core it entrains gas and forms a small molecular outflow (Chernin & Masson 1995).

¹Instituto de Ciencias Nucleares, UNAM, México.

²Institute for Astronomy, Univ. of Hawaii, USA.

³Space Telescope Science Institute, USA.

HH 34 moves away from the driving source with a velocity of about 300 km/s at an angle of roughly 25° to the plane of the sky (Heathcote & Reipurth 1992, Eisloffel & Mundt 1992), values that have been confirmed and refined with subsequent HST images obtained over longer timescales (Reipurth et al. 2002, Raga et al. 2012a).

Devine et al. (1997) showed that the components of the giant HH complex slow down with distance and come to almost a stand-still at the terminal bow shocks. Physical conditions along the jet have been studied by e.g. Morse et al. (1992, 1993), Takami et al. (2006), Beck et al. (2007), García López et al. (2008), Rodríguez-González et al. (2012), and Nisini et al. (2016). The shocks within the HH 34 jet have been successfully modelled as resulting from multi-mode variable velocity flows (Raga & Noriega-Crespo 1998). Refined models have been presented by Raga et al. (2002a, b, 2011b, c, 2012b) and Raga & Noriega-Crespo (2013).

The optical images of the HH 34 complex show that the jet is one-sided, but using Spitzer data Raga et al. (2011a) concluded that this is due to extinction from the cloud core surrounding the driving source, and they found that a counterjet is detected at infrared wavelengths (see also García López et al. 2008 and Antonucci et al. 2014). In this paper, we discuss the nature of the counterjet based on archival near-infrared HST images which reveal its fine structure.

In particular, we discuss an archival HST image taken with the F160W filter (with a dominant contribution from the [Fe II] $1.64 \mu\text{m}$ line), which shows the northern HH 34 counterjet at higher resolution than the Spitzer $4.5 \mu\text{m}$ image of Raga et al. (2011a). The counterjet emission (in the [Fe II] $1.64 \mu\text{m}$ and H_2 $2.12 \mu\text{m}$ lines) has been previously seen in the long-slit spectra of García López et al. (2008), and in the [Fe II] $1.64 \mu\text{m}$ image of Antonucci et al. (2014).

In § 2, we describe the F160W HST image, as well as the $4.5 \mu\text{m}$ Spitzer image of Raga et al. (2011a). In § 3, we present these two images and determine knot positions along the jet and the counterjet. In § 4, we discuss the lateral offsets of the knot positions from the jet axis and the 1.5 and $4.5 \mu\text{m}$ intensities as a function of position for the jet and the counterjet. The 4.5 to $1.5 \mu\text{m}$ intensity ratios are then used to estimate the visual extinction to the knots along the HH 34 jet and counterjet. Finally, the results are summarized in § 5.

2. THE OBSERVATIONS

In this paper we analyze an archival HST image of HH 34 obtained under proposal 11548 (P.I. Thomas Megeath) in October 2009. This image was taken with the F160W filter on the WFC3 camera, with a 2946 s exposure. The F160W filter has a $1.5369 \mu\text{m}$ pivot wavelength and a $0.0826 \mu\text{m}$ RMS bandwidth. For the HH 34 jet, the emission in the F160W filter bandpass is dominated by the [Fe II] $1.64 \mu\text{m}$ line, with a smaller contribution (at $\approx 10\%$) from the [Fe II] $1.60 \mu\text{m}$ line, as shown by the spectroscopic observations of García López et al. (2008). This image has an angular resolution of $\approx 0.1''$.

In order to obtain a calibrated [Fe II] $1.64 \mu\text{m}$ map, we multiply the original HST image by the “PHOTFLAM” parameter (in the header of the fits file) and by the $0.268 \mu\text{m}$ “rectangular passband width” of the F160W filter. This width is given in the WFC3 Instrument Handbook.

We compare the F160W image with the $4.5 \mu\text{m}$ Spitzer image of Raga et al. (2011a). This image is a 6×6 array (with a total integration time of 30 s per pixel) obtained with Channel 2 of the IRAC camera. This channel covers from approximately 4 to $5 \mu\text{m}$, and includes three relatively bright, purely rotational H_2 lines. This image has an angular resolution of $\approx 2''$.

3. THE 1.5 AND $4.5 \mu\text{m}$ EMISSION OF THE HH 34 OUTFLOW

The left frame of Figure 1 shows the $1.5 \mu\text{m}$ image of a region around the source of the HH 34 outflow. It is clear that the counterjet is detected. The central frame of Figure 1 shows a convolution of this image with a $\sigma = 6$ pix ($0.54''$) half-width “Mexican hat” wavelet (see Raga et al. 2017), in which the relatively smooth emission/reflection within $\approx 30''$ from the source is eliminated, so that the jet and counterjet knots are seen more clearly. The right frame of Figure 1 shows the $4.5 \mu\text{m}$ image, with a vertical (7 pixel wide) strip in which the background emission has been subtracted (by carrying out linear interpolations between the intensities on the left and right edges of the strip, as described by Raga et al. 2011a).

In the central frame of Figure 1 (showing the $1.5 \mu\text{m}$ image convolved with a $\sigma = 6$ pix = $0.54''$ half-width wavelet) we have identified the knots along the jet following Reipurth et al. (2002). For the knots along the counterjet, we have used the letters

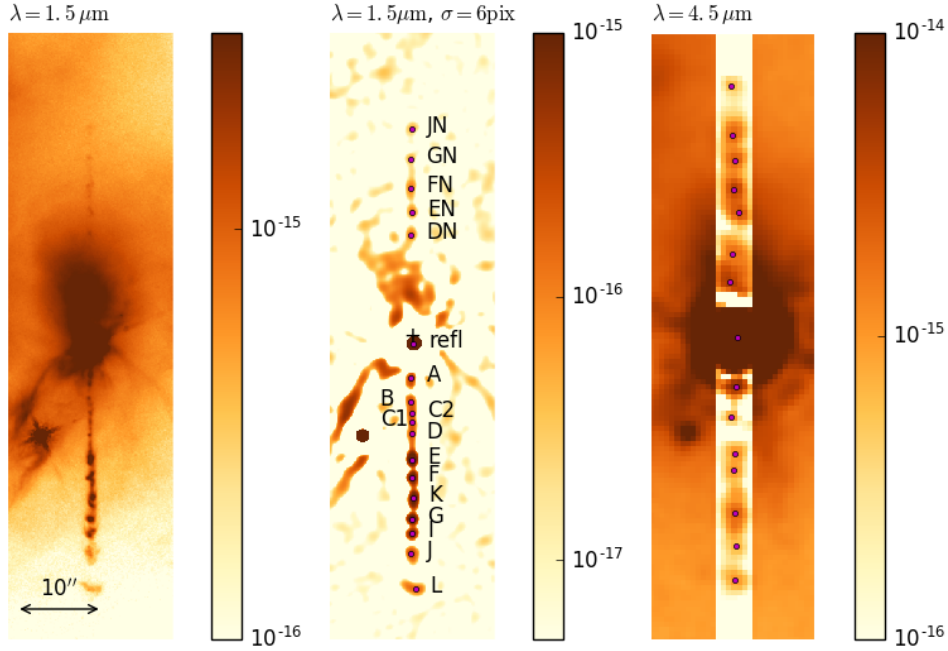


Fig. 1. The HH 34 jet/counterjet system, rotated (14° , counterclockwise) so that the outflow axis is parallel to the ordinate. Left: HST $1.5 \mu\text{m}$ image. Center: $1.5 \mu\text{m}$ image convolved with a 6 pixel ($0''.54$) half-width wavelet. Right: Spitzer $4.5 \mu\text{m}$ image, with a central band in which a linear background (tied to the fluxes at the edges of the band) has been subtracted. In the central and right frames we show the positions of the fitted intensity peaks; the identifications of the peaks are given only in the central frame. The position of the outflow source is shown with a cross in the central frame. The images are displayed with a logarithmic scale on the right of each frame (in units $\text{erg cm}^{-2} \text{s}^{-1} \text{arcsec}^{-2}$). The color figure can be viewed online.

of the jet knots at similar distances from the outflow source, followed by a “N” (to indicate that they belong to the N counterjet).

The knot along the outflow axis closest to the outflow source (labeled “refl” in Figure 1) corresponds to the reflection nebula at the base of the HH 34 jet. The position of the VLA source of Reipurth et al. (2000a), shown with a cross (in the central frame of Figure 1) is $\approx 1''$ to the N of the reflection nebula. This radio source most probably coincides with the position of the outflow source.

4. THE KNOT POSITIONS AND INTENSITIES

We have determined the positions and intensities of the knots along the HH 34 jet and counterjet by fitting paraboloids to the intensity peaks along the outflow axis. The resulting knot positions are shown on the central ($1.5 \mu\text{m}$) and right ($4.5 \mu\text{m}$) panels of Figure 1.

Figure 2 shows the (x, y) positions of the $1.5 \mu\text{m}$ knots, where x is the distance from the outflow source along the flow axis (with $x < 0$ for the jet and $x > 0$ for the counterjet), and y is the distance

perpendicular to this axis (with positive y to the W). From this figure, we note several interesting features:

- the $4.5 \mu\text{m}$ jet and counterjet show almost coincident knots at distances $< 15''$ from the source, and somewhat larger offsets in the jet/counterjet knot positions at larger distances. This effect was described in detail by Raga et al. (2011a, c),
- for $x > 12''$ we see reasonable position coincidences between the 1.5 and $4.5 \mu\text{m}$ jet and counterjet knots. Offsets of $\approx 1''$ in the jet/counterjet directions (with the $1.5 \mu\text{m}$ knots always at larger distances from the source) probably correspond to the proper motions of the knots during the time-interval between the two frames (see § 2),
- for $x \leq 12''$ there are no clear correspondences between the 1.5 and $4.5 \mu\text{m}$ knots.

Also, the $1.5 \mu\text{m}$ knots have systematic displacements, with the knots at $\approx 20''$ from the source showing $y \approx 0.1''$ for the jet and $y \approx -0.1''$ offsets for the counterjet. These (somewhat marginal)

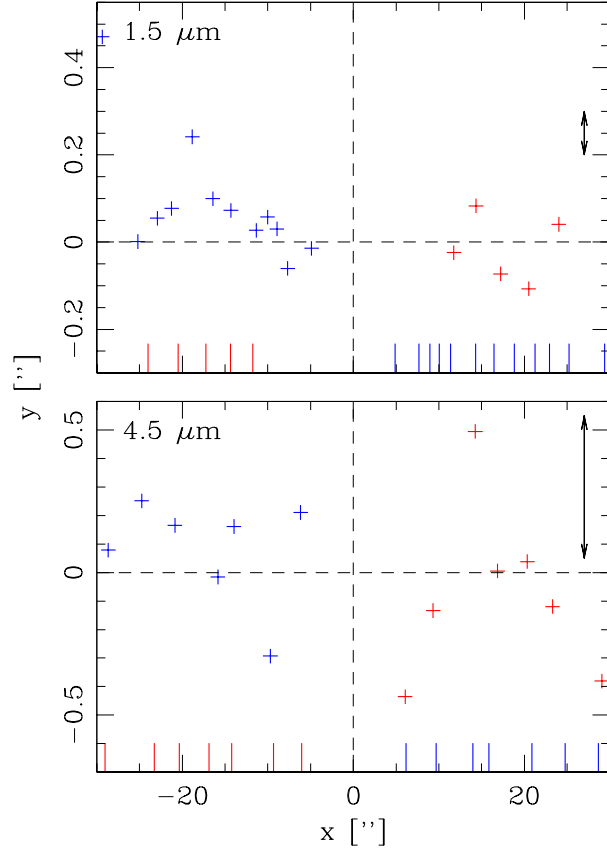


Fig. 2. Offsets perpendicular to the outflow axis as a function of distance from the source measured in the convolved $1.5 \mu\text{m}$ (top) and in the $4.5 \mu\text{m}$ frame (bottom). The blue crosses correspond to the southern jet (negative x values), and the red crosses to the northern counterjet ($x > 0$). Positive y values denote offsets to the W of the outflow axis. The blue (jet) and red ticks (counterjet) along the bottom axis show the positions of the knots along the oppositely directed outflow lobes. The double arrows on the right of the plots show the errors in the offsets. The color figure can be viewed online.

“point symmetric” offsets could indicate the presence of a precession of the outflow axis. At $4.5 \mu\text{m}$ we do not see any systematic offsets of the knots (perpendicular to the outflow axis), as a direct result of the lower angular resolution of this image.

Figure 3 shows the intensities of the jet and counterjet knots in the $1.5 \mu\text{m}$ convolved frame (top) and in the $4.5 \mu\text{m}$ frame (bottom) as a function of distance from the outflow source. The $1.5 \mu\text{m}$ emission shows that:

- the jet knots start at $x \approx 4.5''$, have low intensities with $I_{1.5} \approx 8 \times 10^{-16} \text{erg s}^{-1} \text{cm}^{-2} \text{arcsec}^{-2}$ values for $x < 12''$, and high $I_{1.5} \approx$

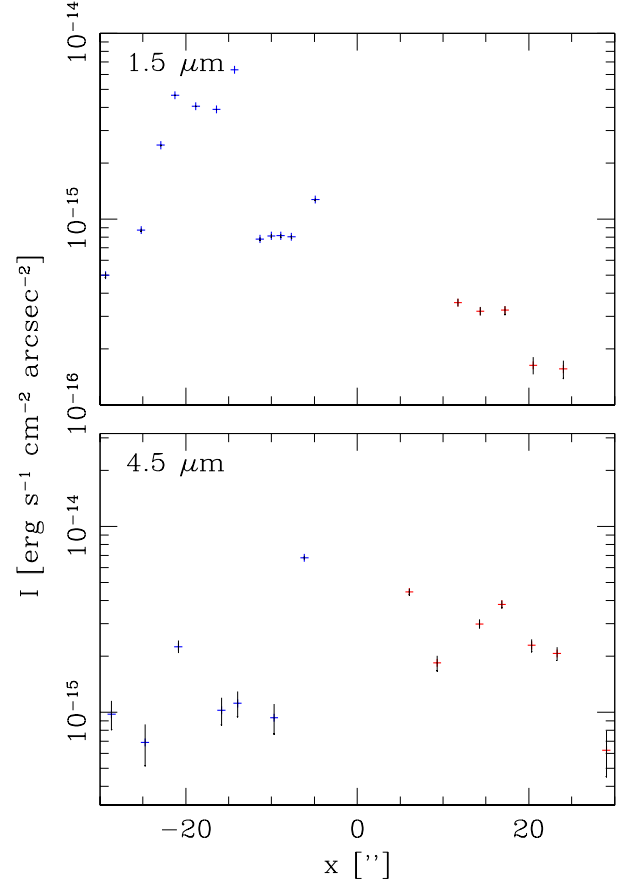


Fig. 3. Peak intensities of the knots along the jet (negative x , blue crosses) and counterjet (positive x , red crosses) in the convolved $1.5 \mu\text{m}$ (top) and in the $4.5 \mu\text{m}$ frame (bottom). The color figure can be viewed online.

$5 \times 10^{-15} \text{erg s}^{-1} \text{cm}^{-2} \text{arcsec}^{-2}$ values for $12 < x < 22''$. At larger distances from the source, the knot intensities drop monotonically with increasing x ,

- the counterjet knots start at $x \approx 11''$, have $I_{1.5} \approx 3 \times 10^{-16} \text{erg s}^{-1} \text{cm}^{-2} \text{arcsec}^{-2}$ values for $x < 20''$ and lower intensities at larger x .

The lack of counterjet knots and low jet knot intensities close to the source (at $x < 11''$) can be interpreted as evidence for a high extinction circumstellar region. Also, the large contrast between the jet and counterjet emission for $x > 11''$ might be due to the presence of a high extinction cloud covering the counterjet.

The $4.5 \mu\text{m}$ emission (bottom frame of Figure 3) shows that:

- the jet and counterjet knots start at a distance $x \approx 6''$ from the outflow source,

- the jet/counterjet knots at similar distances from the source have intensities that differ by factors of at most 3, with brighter knots in the jet or in the counterjet at different values of x .

We now assume that the 4.5 to 1.5 μm intrinsic intensity ratio has the same value for all of the jet/counterjet knot pairs (grouping into pairs the jet and counterjet knots with similar distances to the outflow source) at distances larger than $10''$ from the source (i.e., excluding the first two knots along the jet and the counterjet seen in the bottom frames of Figures 2 and 3). We additionally assume that the $|x| > 10''$ knots of the jet do not have a substantial extinction at 4.5 and 1.5 μm , which is consistent with the relatively low $A_v \approx 1.3$ optical extinction determined (from optical line ratios) by Podio et al. (2006) for this region. We then compare the counterjet and jet 4.5/1.5 μm ratios of the knots (at similar distances from the source, assuming that the knot pairs have the same intrinsic 4.5/1.5 μm ratios) to compute the extinction towards the counterjet knots.

For the jet knots within $10''$ from the source, we assume that the intrinsic 4.5/1.5 μm ratios are constant, with values equal to the 4.5/1.5 μm ratio of knot D (at $x \approx -16''$, see Figures 1-3). With this assumption, we can then compute the extinction towards the jet knots within $10''$ from the outflow source.

In order to convert the “observed vs. intrinsic” 4.5/1.5 μm ratios to a visual extinction A_v , we use an $R = A_v/E(B-V) = 5$ extinction curve, as appropriate for star formation regions (see, e.g., Olofsson and Oloffson 2010). We take this extinction curve from Fitzpatrick (1999), who presents similar results to the ones of Cardelli et al. (1989).

The results of this exercise are given in Figure 4 (where we show the extinction obtained for the southern jet with negative x and for the northern counterjet with positive x). To derive the plotted values we have set $A_v = 0$ for the jet knots with $x < -10''$.

In Figure 4 we see the following:

- there is a region within $\approx 5''$ from the source with no detected emission. This region is likely to have very high extinction,
- as we approach the source along the jet (with $x < 0$), we see a fast growth in A_v as we get within $\approx 10''$ from the outflow source,
- as we move away from the source along the counterjet (for $x > 0$), we see a plateau with $A_v \approx 24 \rightarrow 27$ (comparable to the higher A_v

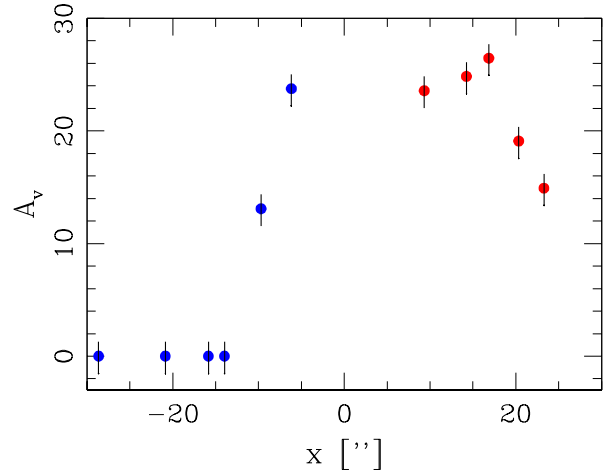


Fig. 4. Optical extinction A_v (calculated from the 1.5 and 4.5 μm intensities, as described in the text) as a function of distance x from the outflow source. The region of the southern jet is shown with negative x values, and the northern counterjet with positive x . The color figure can be viewed online.

value seen in the jet), and then a rapid fall in A_v for $x > 18''$.

We note that Podio et al. (2006) used optical and near-IR diagnostics to obtain an $A_v \approx 1.3$ extinction for the HH 34 jet knots at larger distances from the source, and a higher $A_v \approx 7$ value for the knots closest to the outflow source. This result is qualitatively consistent with the rise in A_v towards the source that we obtain from the 4.5 to 1.5 μm intensity ratios. Also, Reipurth et al. (2000b) determined a rapid rise of A_v when approaching within $\approx 10''$ from the outflow source for the HH 1 jet, which is again qualitatively consistent with our results for the HH 34 jet.

5. CONCLUSIONS

We present a previously unpublished HST 1.5 μm archival image that shows the HH 34 jet and counterjet. This is the first time that we can see the structure of the HH 34 counterjet at $\approx 0.1''$ resolution. We have compared this image with a 4.5 μm Spitzer image of this outflow (which has a lower, $\approx 2''$ resolution, see Raga et al. 2011a).

A comparison of the positions of the jet and counterjet knots shows that in the lower resolution 4.5 μm image we do not see significant offsets from the outflow axis. However, in the new, higher resolution 1.5 μm image we see systematic offsets which indicate (somewhat marginal) point-symmetric jet/counterjet curvatures (see Figure 2).

This result implies that we are probably seeing the effect of a small precession of the outflow axis.

We also measure the intensities of the knots along the jet and counterjet in the 1.5 and 4.5 μm images. We find that at 4.5 μm the knots at similar distances along the jet and counterjet have intensities that differ by at most a factor of ≈ 3 (with brighter counterjet knots at distances $x \approx 10 \rightarrow 18''$ from the outflow source). At 1.5 μm , the jet knots are systematically brighter than the counterjet knots (at similar distances from the source) by factors of $\approx 10 \rightarrow 20$, with the counterjet not being detected for $x < 10''$. This result is likely to be an effect of higher extinction towards the counterjet.

The fact that the jet and counterjet show highly symmetric structures at 4.5 μm (Raga et al. 2011a), while the HH 34 system shows a “one sided” jet at optical wavelengths (with an invisible counterjet that reappears at the HH 34N “head”, see Bührke et al. 1988), indicates that a strong asymmetry in the extinction towards the jet and the counterjet is present.

We have then computed the relative extinction between the jet and the counterjet assuming that the intrinsic 1.5 to 4.5 μm ratios have identical values for the jet and counterjet knots at similar distances from the outflow source. With this assumption (and using an appropriate extinction curve) we have calculated the visual extinction A_v along the HH 34 jet and counterjet.

We find that, approaching the outflow source along the southern jet, A_v grows quite dramatically within $\approx 10''$ from the source (see Figure 4). This rapid increase in A_v (for decreasing distances from the source) is consistent with the result obtained by Podio et al. (2006) from optical and near-IR diagnostics of the HH 34 jet.

Moving away from the source along the northern lobe of the outflow, the counterjet emission is first detected at $\approx 5''$ from the source at 4.5 μm , and then at $\approx 10''$ from the source at 1.5 μm (see Figure 3). For larger distances from the source (where we detect the counterjet at both 1.5 and 4.5 μm), we obtain an extinction with $A_v \approx 24 \rightarrow 27$ out to $\approx 17''$, followed by a strong decrease to $A_v \approx 15$ (at $\approx 23''$ from the source, see Figure 4).

We therefore see the existence of:

- a very high extinction region within $\approx 10''$ from the source, with a steep rise in A_v along the jet towards the outflow source, and an undetected counterjet within $\approx 5''$ from the source,
- a plateau in the extinction along the counterjet from $\approx 10''$ (where the counterjet first appears

in the 1.5 μm image) out to $\approx 17''$ to the N of the outflow source, followed by a sharp decrease in A_v at larger distances.

It then appears that we see evidence for the existence of two structures that produce the extinction:

- a central core with a $\approx 10''$ radius,
- a spatially more extended, dense structure in the foreground of the counterjet.

This extended structure could be related to the complex molecular emission observed in the region around the HH 34 outflow (see, e.g., Stapelfeldt & Scoville 1993 and Anglada et al. 1995).

Our determination of the extinction, however hinges on an assumed symmetry between the 4.5/1.5 μm ratios of the jet and counterjet knots with $|x| > 10''$, and an assumed constancy of this ratio for the $|x| < 10''$ jet knots. The precision of our position-dependent A_v determination is therefore quite questionable!

A more precise measurement of the extinction in the HH 34 jet and counterjet will be obtained with future James Webb Space Telescope observations of this outflow system. These observations will provide the IR diagnostic lines appropriate for carrying out a proper determination of the position-dependent extinction.

AR acknowledges support from the DGAPA-UNAM grant IG100218. We thank an anonymous referee for relevant corrections.

REFERENCES

- Anglada, G., Estalella, R., Mauersberger, R., et al. 1995, *ApJ*, 443, 682
- Antoniucci, S., La Camera, A., Nisini, B., et al. 2014, *A&A*, 566, A129
- Bally, J. & Devine, D. 1994, *ApJ*, 428, L65
- Beck, T. L., Riera, A., Raga, A. C., & Reipurth, B., 2007, *AJ*, 133, 1221
- Bührke, T., Mundt, R., & Ray, T. P. 1988, *A&A*, 200, 99
- Cabrit, S. & Raga, A. C. 2000, *A&A*, 354, 667
- Cardelli, J. A., Clayton, G. C., & Mathis, J. S. 1989, *ApJ*, 345, 245
- Chernin, L. M. & Masson, C. R. 1995, *ApJ*, 443, 181
- Davis, C. J. & Dent, W. R. F. 1993, *MNRAS*, 261, 371
- Devine, D., Bally, J., Reipurth, B., & Heathcote, S. 1997, *AJ*, 114, 2095
- Eisloffel, J. & Mundt, R. 1992, *A&A*, 263, 292
- Fitzpatrick, E. L. 1999, *PASP*, 111, 63
- García López, R., Nisini, B., Giannini, T., et al. 2008, *A&A*, 487, 1019
- Heathcote, S. & Reipurth, B. 1992, *AJ*, 104, 2193

- Kounkel, M., Hartmann, L., Loinard, L., et al. 2017, ApJ, 834, A142
- Masciadri, E., de Gouveia Dal Pino, E. M., Raga, A. C., & Noriega-Crespo, A. 2002, ApJ, 580, 950
- Menten, K. M., Reid, M. J., Forbrich, J., & Brunthaler, A. 2007, A&A, 474, 515
- Morse, J. A., Hartigan, P., Cecil, G., & Raymond, J. C. 1992, ApJ, 399, 231
- Morse, J. A., Heathcote, S., Hartigan, P., & Cecil, G. 1993, AJ, 106, 1139
- Nisini, B., Giannini, T., Antonucci, S., et al. 2016, A&A, 595, A76
- Olofsson, S. & Olofsson, G. 2010, A&A, 522, A84
- Podio, L., Bacciotti, F., Nisini, B., et al. 2006, A&A, 456, 189
- Raga, A. C. & Mateo, M. 1988, AJ, 95, 543
- Raga, A. C. & Noriega-Crespo, A. 1998, AJ, 116, 2943
- _____. 2013, RMxAA, 49, 363
- Raga, A. C., Velázquez, P. F., Cantó, J., & Masciadri, E. 2002a, RMxAA, 38, 251
- _____. 2002b, A&A, 395, 647
- Raga, A. C., Noriega-Crespo, A., Lora, V., et al. 2011a, ApJ, 730:L17
- Raga, A. C., Noriega-Crespo, A., Kajdic, P., et al. 2011b, RMxAA, 47, 277
- Raga, A. C., Noriega-Crespo, A., Rodríguez-Ramírez, J. C., et al. 2011c, RMxAA, 47, 289
- Raga, A. C., Noriega-Crespo, A., Rodríguez-González, A., et al. 2012a, ApJ, 748, 103
- Raga, A. C., Rodríguez-González, A., Noriega-Crespo, A., & Esquivel, A. 2012b, ApJ, 744, L12
- Raga, A. C., Reipurth, B., Esquivel, A., et al. 2017, RMxAA, 53, 485
- Reipurth, B. & Heathcote, S. 1992, A&A, 257, 693
- Reipurth, B., Chini, R., Krügel, E., et al. 1993, A&A, 273, 221
- Reipurth, B., Bally, J., Graham, J. A., et al. 1986, A&A, 164, 51
- Reipurth, B., Yu, K. C., Heathcote, S., et al. 2000a, AJ, 120, 1449
- Reipurth, B., Heathcote, S., Yu, K. C., et al. 2000b, ApJ, 534, 317
- Reipurth, B., Heathcote, S., Morse, J., Hartigan, P., & Bally, J. 2002, AJ, 123, 362
- Rodríguez, L. F. & Reipurth, B. 1996, RMxAA, 32, 27
- Rodríguez, L. F., Reipurth, B., & Chiang, H.-F. 2014, RMxAA, 50, 285
- Rodríguez-González, A., Esquivel, A., Raga, A. C., et al. 2012, AJ, 143, 60
- Stapelfeldt, K. R. & Scoville, N. Z. 1993, ApJ, 408, 239
- Takami, M., Chrysostomou, Ray, T. P., et al. 2006, ApJ, 641, 357

- A. Noriega-Crespo: Space Telescope Science Institute, 3700 San Martin Drive, Baltimore, MD 21218, USA.
- A. C. Raga: Instituto de Ciencias Nucleares, Universidad Nacional Autónoma de México, Ap. 70-543, 04510 Ciudad de México, México (raga@nucleares.unam.mx).
- B. Reipurth: Institute for Astronomy, University of Hawaii at Manoa, Hilo, HI 96720, USA.